Mine Water Environ (2018) 37:423–430
DOI 10.1007/s10230-017-0483-z

TECHNICAL ARTICLE

Dynamic Monitoring of Water in a Working Face Floor Using 2D Electrical Resistivity Tomography (ERT)

Weifu Gao[1] · Longqing Shi[1] · Jin Han[2] · Peihe Zhai[1]

Received: 2 December 2016 / Accepted: 11 August 2017 / Published online: 8 September 2017

Abstract The roof and floor of a water-rich area can be explored using traditional two-dimensional (2D) electrical resistivity tomography (ERT), but this method cannot be applied to a water-rich internal working face. In this paper, the resistivity of an internal working face was determined using 2D ERT by laying electrodes and cables in two adjacent roadways and using an equatorial dipole device. The water inrush process of the goaf floor in the study area was monitored with pre-implanted electrodes and cables at the front of the mining working face and was analyzed using the processed results of four acquired data sets. The location of the water inrush from the floor was determined based on the change in the resistivity of the floor and the hydrological variations at the observational hole, which provided the basis for how to stop the water inrush.

Keywords Dipole equatorial array · Liangzhuang coal mine · Water inrush of the goaf floor · Location of water-inrush from floor

Introduction

With China's rapid economic development, most shallow coal deposits have been mined; therefore, more attention is being paid to deeply buried coal seams. In the Northern China type coal fields (Fig. 1a), Carboniferous and Permian coal seams were mostly directly deposited on the Ordovician limestone, and Silurian and upper Devonian strata are absent. The Ordovician limestone developed extensive underground karst systems due to extreme weathering and erosion that spanned approximately 900 million years. Since the Carboniferous coal seams are close to the Ordovician limestone and the area has been subjected to tectonic action, most of the karst features of the Xujiazhuang limestone floor tends to resemble those of the Ordovician limestone. There is a water-resisting layer (an aquiclude) between the aquifer and the coal floor. If the water pressure is greater than the resisting capability of the layer, water inrush from the floor will occur. Therefore, the potential risk of a karst water inrush into the mine is considerable.

The North China type coalfield is generally divided into the Carboniferous Taiyuan formation and the Permian Shanxi formation. The Permian coal seam is relatively shallow and is generally called the upper coal seam. The Carboniferous coal seam is relatively deep and is called the lower coal seam. The process of mining the lower seam is hampered by the high water pressure in the underlying Ordovician limestone, which leads to large amounts of water seeping into the mine, which can easily flood the working face. For safety, mining is generally conducted from the front to the rear. First, a roadway is opened up far into the planned mining area; the mined face is called the working face. This layout significantly influences the mining process.

Two types of exploration methods are generally used: drilling and geophysical methods. The drilling method is characterized by accurate exploration, relatively low efficiency, and high costs, while geophysical methods are also accurate, but are more efficient and less expensive. Thus, geophysical methods are favored. However, accurately assessing the amount of water in the rocks is a problem with

✉ Longqing Shi
857401763@qq.com

[1] College of Earth Sciences and Engineering, Shandong University of Science and Technology, Qingdao 266590, China

[2] College of Information Sciences and Engineering, Shandong University of Science and Technology, Qingdao 266590, China

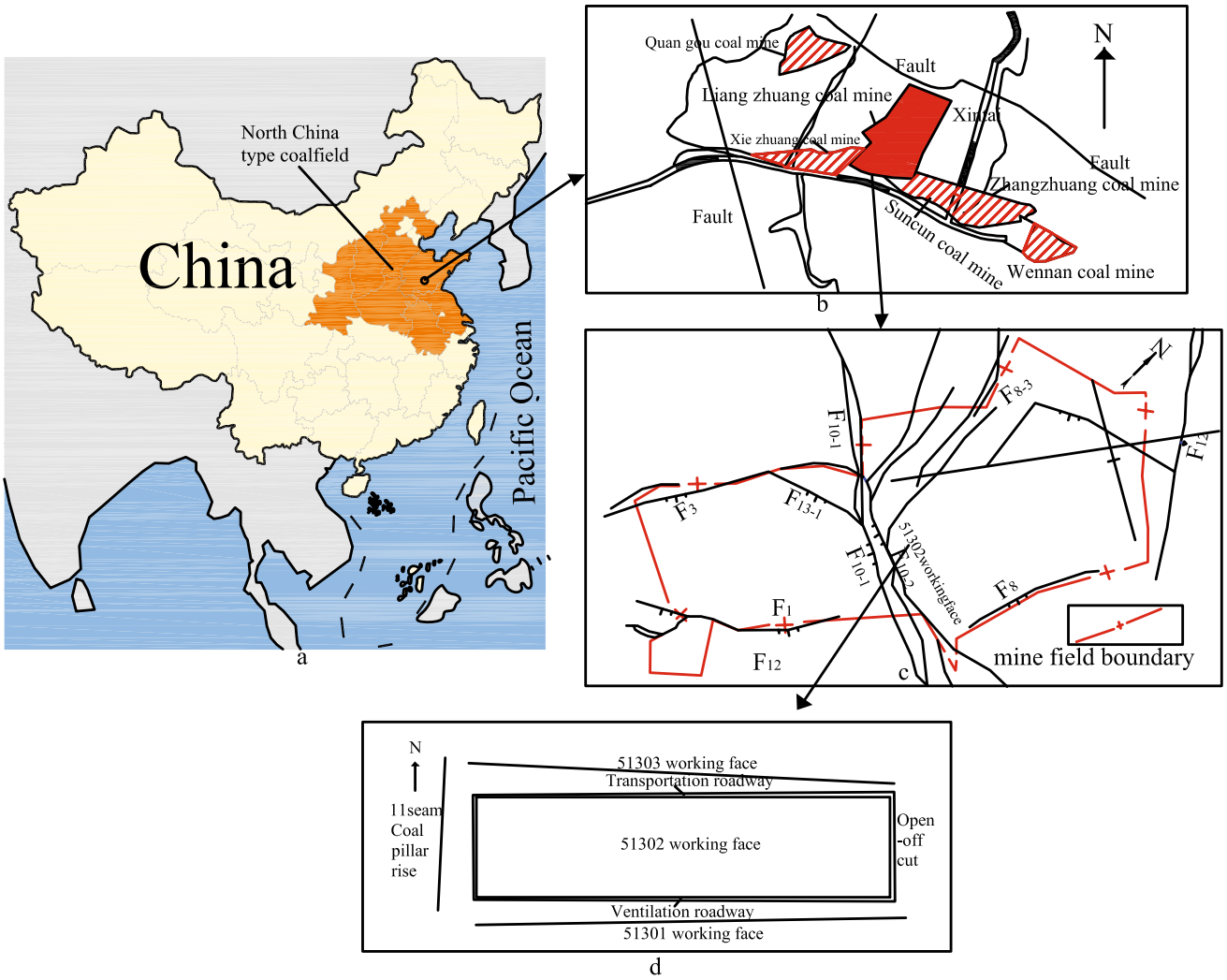

Fig. 1 Map of the study area; Location of North China type coalfields (**a**); Location of the Liangzhuang coal mine (**b**); Location of the 51302 working face (**c**); Schematic diagram of the 51202 working face (**d**)

existing equipment. Therefore, selecting suitable and efficient geophysical prospecting methods to detect the occurrence and migration of water in the working face floor is a matter of some urgency.

Two-dimensional (2D) electrical resistivity tomography (ERT) integrates electric sounding and profiling methods for array exploration, and was introduced in China in the late 1980s. Han et al. (1997) successfully brought 2D ERT to the mines and applied it to detect hidden water inrush structures at the working face. The theoretical formula of Yue and Li (1999) permitted spatial data correction, he laid the foundation for 2D ERT of accurate data in mine. The way of 2D ERT of parallel data acquisition was used downhole (Cao 2008; Liu et al. 2009; Wu et al. 2010) to detect water-rich floor strata, and improved data collection efficiency. Loke and Barker (1995) took up resistivity inversion with the least squares method, while Wu et al. (2010) did the same inversion using the conjugate gradient method, which improved the operational speed of the three-dimensional (3D) inversion. The development of inversion software laid the foundation for 3D exploration. Yutaka (1994) used the finite difference method to carried out 3D inversion studies and found that 3D resistivity surveys results were better than those of 2D. Therefore, 3D exploration has become the current trend in development. Shi et al. (2009) proposed the 3D mine DC method, which has been continuously improved and is well known in the Xinwen, Feicheng, and southwestern Shandong mine areas. Liu et al. (2012) achieved real-time monitoring of the water inrush process in roadways by combining 3D resistivity with the constraint resistivity method. Some unconventional 3D observational systems were adopted in urban zones (Chavez 2015; Tejero-Andrade et al. 2015), where they achieved good results. Although 3D inversion can provide information on water abundance in

external rock strata, it is static and cannot show floor water dynamics.

Based on the previous studies, we placed electrodes and cables into two roadways of a working face, with the cable plugs outside of the working face and connected to the data acquisition instrument. Then, the dipole equatorial array was used to determine the permanent rock resistivity in the working face floor (including the goaf). The collected data were preprocessed and inverted to detect the working face's water-rich area. A total of five rounds of data were collected during the mining of the working face, and each result was compared to the previous one to identify changes, and thus monitor the dynamics of the water-rich areas in the working face floor. The key advantage of this method is that other geophysical methods fail to collect data in the goaf.

Study Area

Geological Backgrounds

The 51,302 working face is located in the southeastern section of the 5th mining area in the well field, which is the second coal mining face of the 13th coal seam in the 5th mining area. The 02 represents the face number. The working face is adjacent to the 51,301 stope face above it and the 51,303 stope face (now tunneling) below (Fig. 1d). The average (working face length) surface strike is 690 m, while the average (stope width) is 165 m. The working face is a monoclinal structure with small local folds, which have negligible effects on mining, but significantly affects water drainage. The strike of the coal seam is northwestern, inclining to the northeast, with an average angle of 15°. The 13th coal seam belongs to the Carboniferous Taiyuan formation, with a thickness of 1.07–1.60 m, with an average of 1.54 m (Fig. 1d). The average thickness of the pure coal seam is 1.12 m, and the dip angle (the angle between the coal seam surface and the horizontal plane) ranges from 10° to 22°, and averages 16°.

Hydrogeological Conditions

The mining elevation of the 51,302 working face is −580 m. The no. 13 coal seam being mined has a face length of 165 m. This working face is on a monoclinal structure with a small local fold that has little effect on its mining. The average thickness of the coal seam is 1.6 m. The dip angle of the coal seam ranges from 10° to 22°, with an average of 11°. The no. 13 coal seam is 12 m above the no. 15 coal seam, 40 m above the Xujiazhuang limestone, and 76 m above the Ordovician limestone.

As shown in Fig. 2, the mining of the 51,302 working face is mainly affected by the 4th limestone, which is its direct roof, and the underlying Ordovician and Xujiazhuang limestone. The 4th limestone contains fissures that produce 9 m^3/h of water in the working faces of the haulage and ventilation roadways and up to 12 m^3/h in the eastern 51,302 working face.

Based on observations during ventilation roadway tunneling in the 51,302 working face, the Xujiazhuang and Cao limestone strata are not strongly water-bearing. However, both formations apparently communicate with the

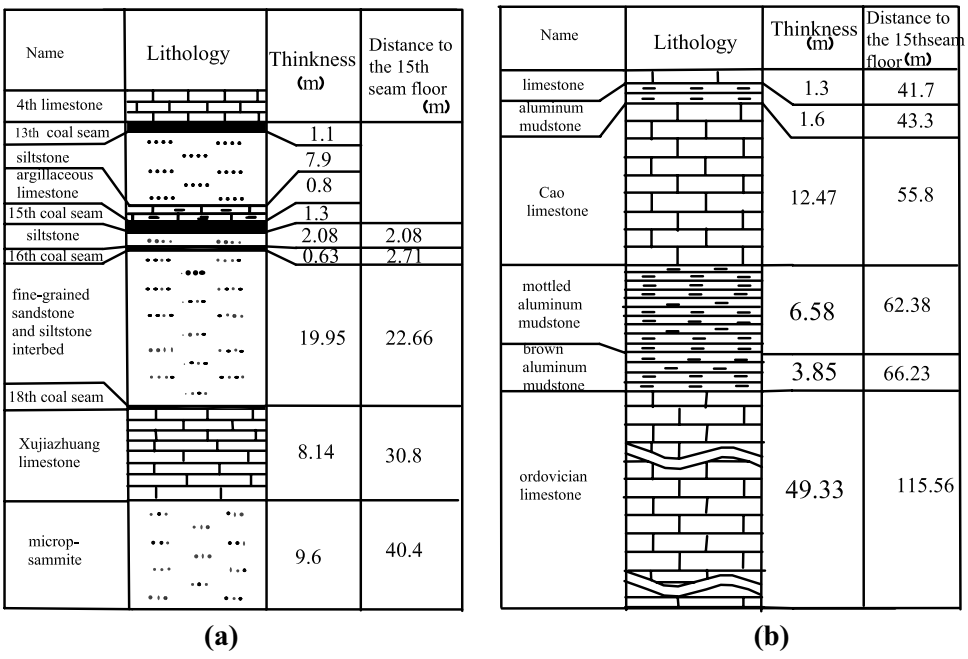

Fig. 2 Strata column of the Liangzhuang coal mine. The top of the strata column (**a**) and the lower part of the strata column (**b**)

Ordovician limestone, which has abundant water at shallow depths, and although it has somewhat less at greater depths, its fractures remain water filled. The Ordovician limestone is characterized with anisotropic and heterogeneous water storage and permeability. Its operating hydrostatic pressure was measured in a borehole as 1.1 Mpa.

Methods

Equatorial Dipole Arrays in the Working Face

The down-hole resistivity method has generally been used in roadways for data acquisition, and can show the resistivity cross-section diagrams for analysis of water in the floor strata. However, water inrush from the seam floor usually occurs within the working face, which makes it critical to detect water-rich areas there. Traditional ERT is 2-dimensional; it can only show the water-rich profile of the tunnel roof and floor strata and is incapable of measuring the water richness of the strata in the working face. Therefore, we used an equatorial dipole array, in which the electrodes and cables were arranged in two roadways, while the measuring points were set in the middle of the working face. This allows rock resistivity data to be collected within the working face for analysis of the water in the floor.

As shown in Fig. 3a, the current electrodes (A) are to the left at the beginning of cable 1, and the other current electrodes are to the left at the beginning of cable 2. The potential electrodes (M) are the 2nd electrodes of cable 1; the potential electrodes (N) are the 2nd electrodes of cable 2; the first big black circles indicate the location of the first measurement. The current electrodes AB remain fixed while the potential electrodes MN simultaneously move away the starting position (the arrows depict the direction of the electrode shift) until the potential electrodes are close the end of the cable. In the next step, the current electrodes, A and B, are moved one electrode position towards the origin, and M and N are located below them. The process then starts all over again. This procedure is repeated until the current and potential electrodes are close to the ends of the cables.

The equatorial dipole array is used on the working face and a section of the face, as shown in Fig. 3b. First, the current electrodes AB are fixed, and then the potential electrodes MN are shifted from the origin of the cable to end. When the potential electrodes M(N) arrived at the end of the cable, a rolling line of measurements was recorded. Then, the current electrodes A (B) are shifted by one electrode position and another rolling line was recorded. According to the above process, more rolling lines were recorded. All of the rolling lines are used to represent a section of the working face.

Observation System

To comply with the design requirements, two 915 m-long high-density underground cables were fabricated. The cable connection is illustrated in Fig. 4. The pins in the 32-core plugs on the cables are connected to taps, from 1 to 30, with a tap spacing of 10.5 m, using orange polyurethane sheaths.

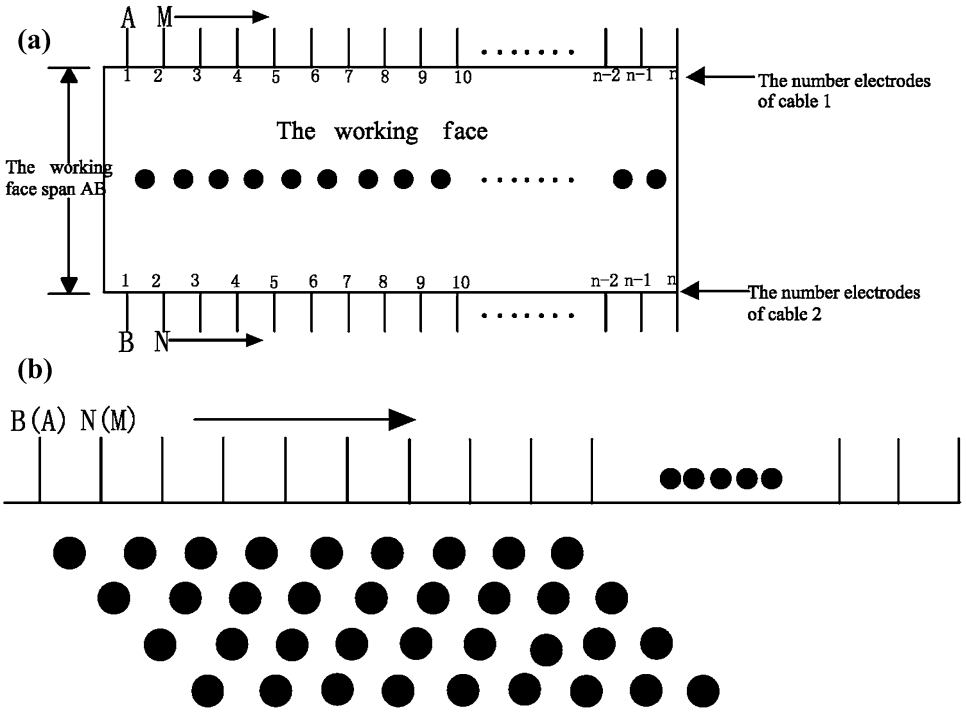

Fig. 3 The data acquisition process is displayed for the Equatorial dipole arrays. Electrodes are showed as *vertical bar*, and *arrows* indicate the diction of the electrodes shifting. The *big black circles* depict the location of resistivity recording points, the *small black circles* are ellipsis. Plan of the Equatorial dipole array on the working face is showed (**a**). The same process is depicted, section of the Equatorial dipole array on the working face (**b**)

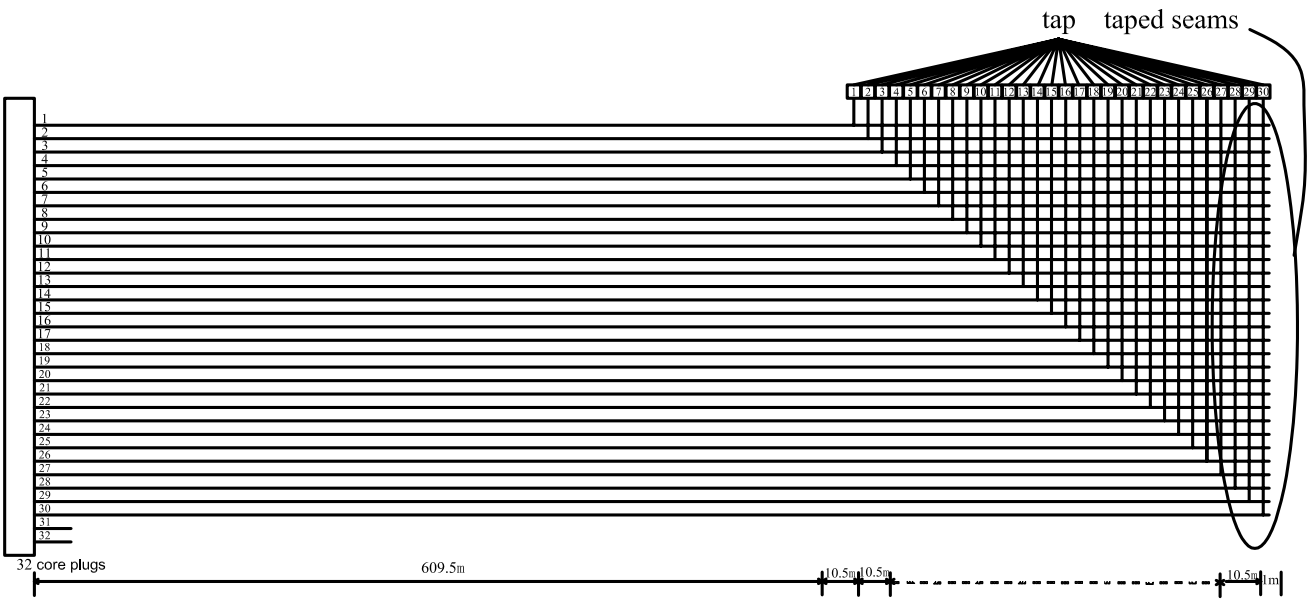

Fig. 4 Connection of cables

Except for the 32-core plug, the cables are sealed to be waterproof, allowing for usage in humid environments. One end of the cable is connected to a core plug, while the other end is sealed using an adhesive. Each tap is run through a 30 cm long multicore copper wire with a cross-sectional area of 0.3 mm^2. The insulation of the core wires should be greater than 500 MΩ (if it is less than 500 MΩ, the cable may leak or cause the measurement signal to be inaccurate).

The underground cable burial work was completed on July 2 and 3, 2005, which included embedding one electrode and one cable in both the top and bottom roads of the 51,302 working face. To ensure optimal configuration of the cables and electrodes and their production, the cables and electrodes were buried at certain depths in trenches. The electrodes were inserted into the electrode hole and sealed with stemming. The requirements for the cable trenches and electrode holes were as follows:

- Cable trench size: 300 mm deep, 200 mm wide. The cable trenches were emplaced in the upper base floor of the upper roadway and the lower base floor of the lower roadway, and inclined along the coal wall direction, close to the coal wall.
- The electrode holes were 28 mm in diameter and 300 mm deep.
- The electrodes were inserted into the electrode hole, and the electrodes holes were then filled with stemming. In addition, the joint of the electrodes and cable connections were all be sealed with the stemming.

Data Acquisition and Processing

After installation of the underground cables on July 3, four rounds of data collection were completed between July 14 and August 7. A total of four cross-sections were acquired using the equatorial dipole devices. Then, the collected data were stored in the WDJD-3 multifunctional digital DC induced polarization instrument, which was transferred by BTW2000 communication software to a workstation. The collected resistivity data required preprocessing, which included topographic correction, filtering, abrupt change point elimination, and averaging/smoothing.

Since the level of the working face ranged from −428.7 to −440.6 m, a topographic correction was necessary. According to electrostatic field theory, topography can cause the measured resistivity to be greater than actual resistivity in convex terrain and smaller than the actual one in concave terrain. Therefore, in order to reflect the actual situation, terrain correction is necessary. When the slope of the convex terrain and the horizontal surface is β, the actual resistivity is $\rho_s = \rho_{\text{mea}} \cdot \cos\beta$; when the slope of concave terrain and the horizontal surface is β, the actual resistivity is $\rho_s = \rho_{\text{mea}} / \cos\beta$, and when ρ_s is the actual resistivity of the concave or convex terrain; ρ_{mea} is the measured resistivity after the mutation point processing.

The construction activities of the field staff led to some random interference, so data processing included filtering, which not only eliminated random high frequency interference but also removed and weakened the vibrating part of the apparent resistivity curve. This simplifies abnormal forms and improves processing accuracy. Abrupt change

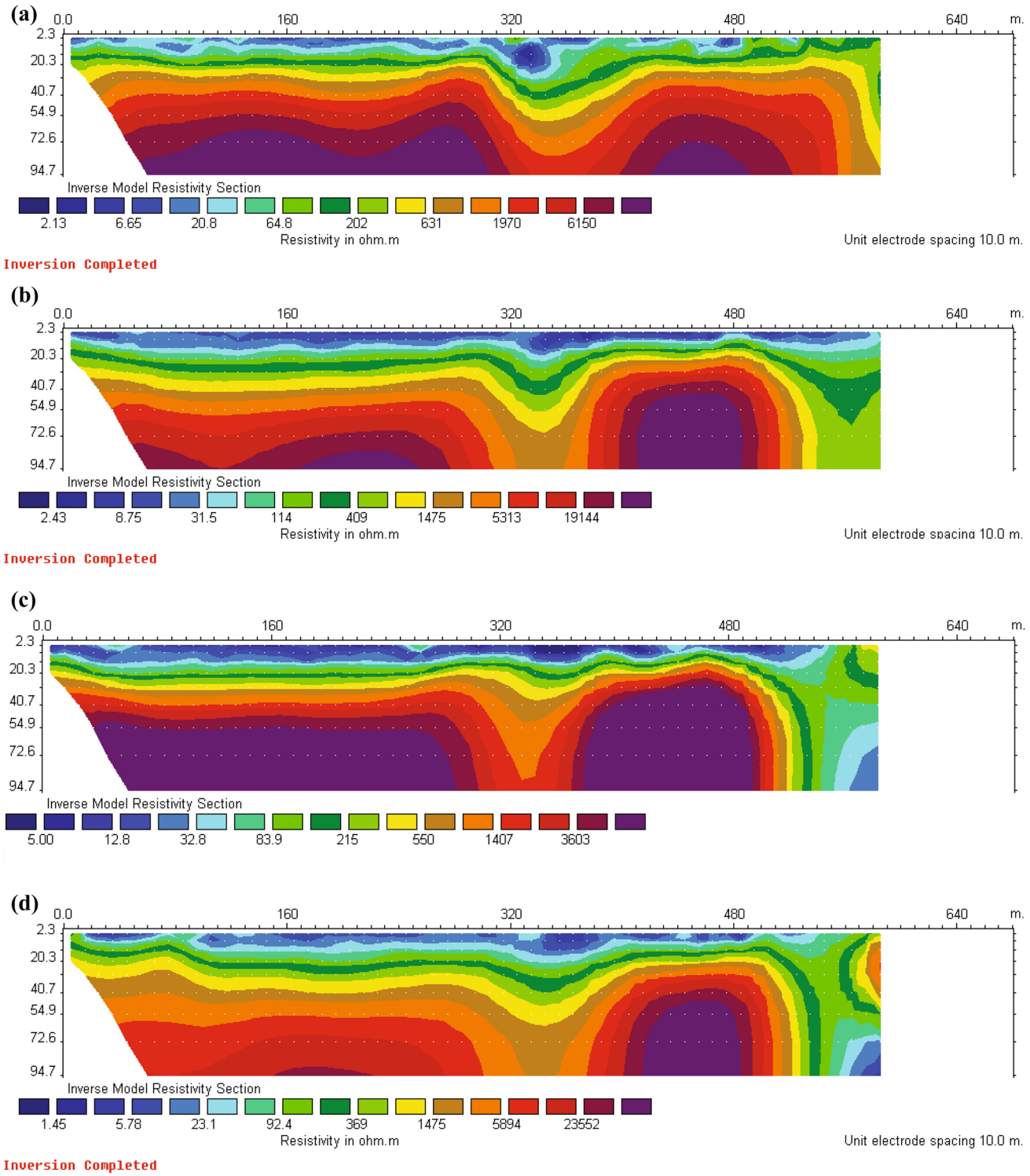

Fig. 5 Electrical resistivity cross-sections for Liangzhuang 51302 working face. The inversion of map on July 14 (**a**); The inversion of map on July 27 (**b**); The inversion of map on August 5 (**c**); The inversion of map August 7 (**d**)

points can emerge during data collection due to bad electrode grounding or metal interference at the collection site, which should be eliminated to reduce its negative effects on the processing results.

The registration points for the data measurement are distributed in their corresponding cross-sections, which can be divided into a number of smaller units. If there are data points within a smaller unit, the apparent resistivity of the

unit is that numerical value. If there are no data points, a cubic spline interpolation will be introduced, in which power or exponential functions will be applied to smooth the data in each unit. If smooth averaging is not carried out, the local range inversion error is too large, and the overall inversion is affected.

After the data were preprocessed, we used RES2D commercial software (Loke 2004) to invert it. The inversion process automatically stopped when the root mean square (RMS) was less than 10%. If this requirement was not reached, the inversion was repeated six times (the default inversion count).

Results and Conclusions

Figure 5a–d are the inversion maps of the mining position at sections x = 570 m, x = 540 m, x = 530 m, and x = 530 m, respectively. By comparing the calculated resistivity change in the x = 540–570 m position (This position is recorded as A region), we can draw the following conclusions: with mining of the working face, in Fig. 5a, the A region began to appear abnormal in certain areas; the calculated resistivity began to decrease. In Fig. 5b, the A region of the abnormal area range expanded further, and the calculated resistivity continued to decrease. In Fig. 5c, the A zone of the abnormal area reached its maximum, and, at the same time, water inrush occurred and the water inrush value reached 30 m^3/min. In Fig. 5d, the abnormal area decreased, and the water inrush value reached 16 m^3/min.

From Fig. 5, the variation of the calculated resistivity of the abnormal area in region A shows that the process of water inrush from the floor is the gradual formation of inrush channels. Figure 5a, b show the development of the inrush channel in the A region and the range of variation in the calculated resistivity of the abnormal area, as seen in Fig. 5c. The range of variation of the calculated resistivity of the abnormal area in the A region shows that the upper low abnormal zone and the lower low abnormal zone are integrated. This indicates that the water channel has formed, leading to inrush through the floor. The fact that inrush occurs proves the correctness of the calculated resistivity variation range of the anomaly area in the A zone in Fig. 5a, b.

We know that after the water inrush, the inrush flow decreased gradually and then gradually stabilized from Fig. 6. After the water inrush, it can be seen from Fig. 7 that the hydraulic pressure in the Ordovician limestone declined. Figures 6 and 7 verified the characteristics of the high hydraulic pressure and the large water inrush channel during the early stage of water inrush from the floor. This is the same as the calculated resistivity anomaly area trend in the A region of Fig. 5c, d. Therefore, the inrush from the floor is a goaf-lagging inrush; the type of inrush is that of the Ordovician limestone water and the location of the inrush channel is in the x = 540–570 m section.

The equatorial dipole devices was adopted to construct a dynamic monitoring system, using the two roadways of a working face before mining to bury electrodes and cables, and has been successfully used to detect anomalous changes in the processes in the working face floor and water inrush processes in the mining goaf. Using the method in this paper, we can determine the water inrush at this working face is goaf-lagging water inrush from the floor; instead, the type is Ordovician limestone karst water inrush, and the location of the water inrush channels are determined to provide information about the water inrush from the floor.

This dynamic floor monitoring system was built on the basis of two-dimensional resistivity. Therefore, it explores only the hydrological changes along the axis position of the span of the working face. To more visually monitor the water regime changes in the work floor, the development of a 3D floor hydrological dynamic monitoring system should be targeted.

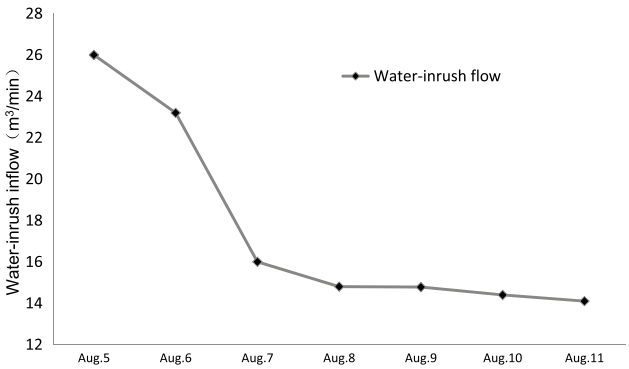

Fig. 6 The change graph of the water-inrush flow at in the Ordovician limestone at hydrological hole 2 after the water inrush

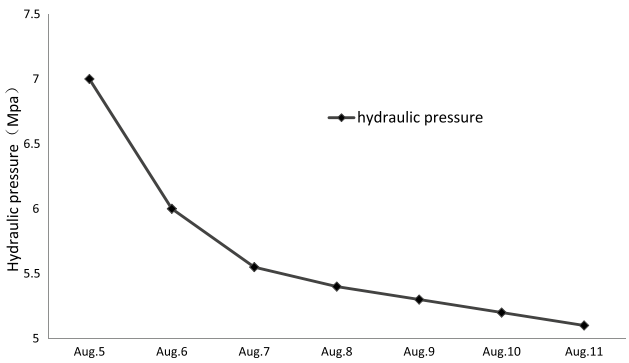

Fig. 7 Change of the hydraulic pressure in the Ordovician limestone at hydrological hole 2 after the water inrush

Acknowledgements The work of the first author was supported by the National Science Foundation (41572244), the Shandong Province Nature Science Fund (ZR2015DM013), and special funds provided by the Taishan Scholars construction projects and the Shandong University of Science and Technology graduate innovation science and technology fund (SDKDYC170212). The authors gratefully acknowledge the anonymous reviewers that substantially improved the manuscript.

References

Cao Y (2008) The imaging technology of concurrent DC method. MSc thesis, Anhui University of Science and Technology, Huainan

Chavez RE (2015) Imaging fractures beneath a residential complex using novel 3D electrical resistivity arrays. J Environ Eng Geophys 20(3):219–233

Han DP, Zhang TM, Shi YD (1997) The principle and interpretation of the monopolar dipole DC penetration at working face. Coal Geol Explor 25(5):32–35

Liu SD, Wu RX, Zhang PS (2009) 3-dimensional parallel electric surveying and its applications water disaster exploration in coal mines. J Chin Coal Soc 34(7):927–932

Liu B, Li SC, Nie LC (2012) Research on simulation of mine water inrush real-time monitoring of using electrical resistivity constrained inversion imaging method. J Chin Coal Soc 37(10):1722–1731

Loke MH (2004) Tutorial: 2-D and 3-D electrical imaging surveys. http://www.geotomosoft.com. Accessed 11 July 2007

Loke MH, Barker RD (1995) Least squares deconvolution of apparent resistivity pseudosections. Geophysics 60(6):1682–1690

Shi LQ, Zhai PH, Wei JC (2009) Application of 3D high density electrical technique in detecting the water enrichment of strata. J Shandong Univ Sci Technol 27(6):1–4

Tejero-Andrade A, Cifuentes G, Chávez RE, López-González AE, Delgado-Solórzano C (2015) L- and corner-arrays for 3D electric resistivity tomography: an alternative for geophysical surveys in urban zones. Near Surf Geophys 13(4):355–367

Wu RX, Liu SD, Zhang PS (2010) The exploration of two gateways parallel 3D electrical technology for water-rich area within coal face floor. J Chin Coal Soc 35(3):454–457

Yue JH, Li ZD (1999) Effect of direct current prospecting in mine roadway. J Chin Coal Soc 24(1):7–10

Yutaka S (1994) 3D Resistivity inversion using the finite-element method. Geophysics 59(12):1839–1848